Langmuir

Article

pubs.acs.org/Langmuir

A Combined Vibrational Sum Frequency Generation Spectroscopy and Atomic Force Microscopy Study of Sphingomyelin−Cholesterol Monolayers

Champika Weeraman, Maohui Chen, Douglas J. Moffatt, Rune Lausten, Albert Stolow,* and Linda J. Johnston*

Steacie Institute for Molecular Sciences, National Research Council of Canada, Ottawa, ON K1A 0R6

Supporting Information

ABSTRACT: A combination of vibrational sum frequency generation spectroscopy and atomic force microscopy is used to study the changes in morphology and conformational order in monolayers prepared from three natural sphingomyelin (SM) mixtures as a function of surface pressure and cholesterol concentration. The most homogeneous SM gave monolayers with well-ordered acyl chains and few gauche defects with relatively small effects of either increasing surface pressure or cholesterol addition. Heterogeneous SM mixtures with a mixture of acyl chain lengths or with significant fractions of unsaturated acyl chains had much larger contributions from gauche defects at low surface pressure and gave increasingly well-ordered monolayers as the surface pressure increased. They also showed substantial increases in lipid chain order after cholesterol addition. Overall, these results are consistent with the strong hydrogen bonding capacity of SM leading to well-ordered monolayers over a range of surface pressures. The changes in acyl chain order for natural SMs as a function of cholesterol are relevant to formation of sphingolipid−cholesterol enriched domains in cell membranes.

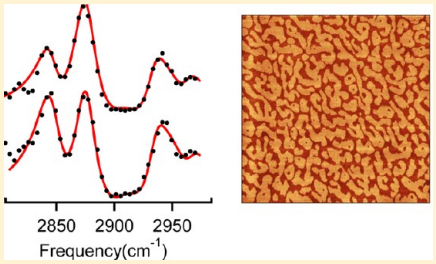

INTRODUCTION

Cell membranes are complex structures with many different lipids and proteins arranged in an asymmetric bilayer. It is now well-recognized that the organization of both lipids and proteins plays an important role in regulating membrane structure and function.[1] Studies of the lipid interactions that determine the properties of biological membranes have frequently used model systems that have a limited number of pure lipid components and can be investigated by a wide range of analytical methods.[2−4] Particular attention has been focused on mixtures of saturated lipids such as sphingomyelins (SM) and phosphatidylcholines (PC) with cholesterol (Chol). Cholesterol has significant effects on the properties of membranes, being an efficient modulator of mechanical strength, fluidity, and phase separation behavior.[5−7] Mixtures of Chol and saturated SMs have been shown to form a liquid-ordered (l_o) phase with properties that are intermediate between those of a gel phase and a fluid or liquid-disordered (l_d) phase. The l_o phase is characterized by high lateral lipid mobility, analogous to a fluid phase, but has a relatively high degree of lipid packing and order, due primarily to the interaction of Chol with saturated long chain sphingolipids. SM-Chol mixtures have been studied extensively as models for membrane rafts in cells.[3,4] The original raft concept postulated that sphingolipid−Chol−protein rich assemblies were found in the plasma membrane and played an important role in biological processes such as cell signaling.[8] During the past 15 years, numerous studies have taken advantage of advances in technologies for studying small lipid and protein domains in order to characterize these elusive membrane domains. Lipid or membrane rafts are now defined as "small (10−200 nm), heterogeneous, highly dynamic, sterol- and sphingolipid-enriched domains that compartmentalize cellular processes. Small rafts can sometimes be stabilized to form larger platforms through protein−protein and protein-lipid interactions."[1,9]

Various analytical methods have been used to examine the interaction of Chol with SM and PC in both monolayers and bilayers.[5−7] The effects of Chol depend on several factors including the lipid headgroup, the chain length, the lipid backbone and the presence of saturated vs unsaturated chains. The condensing effect of Chol on lipid monolayers has been well documented and is defined as the decrease in surface area that occurs upon mixing Chol into PC or SM membranes.[6,10,11] The ordering effect of Chol has been investigated using techniques such as NMR, fluorescence, and electron paramagnetic resonance and can also be evaluated using parameters such as the number of gauche defects or the average tilt angle of the lipid acyl chains. The condensing and ordering effects of Chol on membranes are more pronounced for SM than for saturated PCs with equivalent chain lengths, results that are attributed to the differences in structure between the two phospholipids.[10,11] Specifically, SM can act as both a hydrogen

Received: March 31, 2012
Revised: August 1, 2012
Published: August 13, 2012

Scheme 1

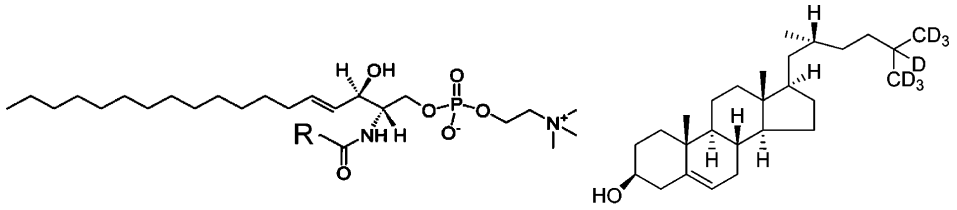

bond donor and acceptor whereas PC can only function as a hydrogen bond acceptor. It is also important to note that Chol is much less effective in condensing unsaturated PCs, one of the main components of natural membranes, relative to either saturated SM or PC.[11]

During the past decade, several groups have shown that the nonlinear optical technique of vibrational sum frequency generation (VSFG) spectroscopy is particularly well suited to probing the order and orientation of lipids in planar membranes such as monolayers and supported lipid bilayers.[12,13] The SFG requirement for a sample that lacks inversion symmetry necessitates the construction of asymmetric bilayers, either by selective incorporation of deuterated lipids in one leaflet or by fabrication of a hybrid bilayer in which the top leaflet is added to a monolayer that is covalently attached to the support. VSFG studies have provided useful information on the order of lipid monolayers or bilayers as a function of membrane additives and preparation conditions, lipid phase transitions, the dynamics for exchange (flip-flop) of lipids between bilayer leaflets, and the orientation of peptides or proteins inserted in lipid membranes.[12−20] Several studies have probed the effects of Chol on saturated PC monolayers and bilayers.[21−25] The CH_3 and CH_2 symmetric stretch vibrations are particularly useful, since the intensity of the CH_3 signal is sensitive to the orientational order of the lipid acyl chains whereas the CH_2 signal intensity increases with increasing gauche defects and is therefore proportional to the conformational disorder in the chains.[21] However, information from VSFG measurements has not yet been correlated with direct measurements of bilayer phase separation.

We have utilized VSFG to probe lipid order for monolayers of three natural SMs and their mixtures with Chol (Scheme 1); the natural SM mixtures provide more relevant models for cellular membranes than the previously studied saturated PCs, since most membrane PCs have one or more unsaturated acyl chains. We used atomic force microscopy (AFM) to image monolayers of the same lipid mixtures, providing useful information on the morphology and phase separation behavior of the monolayers for correlation with VSFG data.[2] Interestingly, we find that the most homogeneous natural SM gives well-ordered monolayers at several surface pressures, as assessed by the relative contributions from the CH_3 and CH_2 symmetric stretch vibrations. By contrast, the more heterogeneous SM mixtures show larger contributions from gauche defects and a larger dependence on surface pressure. Cholesterol addition leads to condensation of the monolayers, increasing the conformational order of the lipid chains, and has a significantly larger effect on the more heterogeneous SM mixtures.

MATERIALS AND METHODS

Materials. Chicken egg sphingomyelin (ESM), porcine brain sphingomyelin (BSM), bovine milk sphingomyelin (MSM), and deuterated cholesterol (cholesterol-25,26,26,26,27,27,27-d_7) were purchased from Avanti Polar Lipids (Alabaster, AL). Methanol and chloroform were from Sigma. The acyl chain distributions for the three natural SMs (RCO in the SM structure in Scheme 1) as provided by Avanti are as follows. ESM: 86% C16:0, 6% C18:0, 3% C22:0 ,and 3% C24:1. BSM: 2% C16:0, 50% C18:0, 5% C20:0, 7% C22:0, 5% C24:0, 21% C24:1, and 10% unknown. MSM: 16% C16:0, 20% C22:0, 34% C23:0, 21% C24:0, 3% C24:1, and 6% unknown. VWR microscope glass slides (1.2 mm thickness) were used for monolayer deposition.

Monolayer Preparation. Monolayers of SM and Chol/SM mixtures (10 and 25 mol % Chol in SM) were prepared by the Langmuir−Blodgett method. Sphingomyelins (egg, milk, and brain) were dissolved in a 5:1 (v/v) methanol/chloroform mixture, and Chol was dissolved in chloroform. Aliquots of SM or SM/Chol mixtures were spread on a Milli-Q water surface at room temperature (22 °C) in a Langmuir−Blodgett trough (Nima 611). The solvent was allowed to evaporate for 20 min prior to compressing the monolayer at a speed of 20 cm^2/min to the desired surface pressure. Monolayer films were deposited on precleaned glass substrates (piranha solution: 3:1 mixture of H_2SO_4 and 30% H_2O_2) or freshly cleaved mica at 3, 15, and 30 mN/m surface pressures at a dip speed of 10 mm/min. Monolayers were air-dried and stored under dry nitrogen until used for either VSFG or AFM experiments. In order to test for lipid oxidation, some monolayers were prepared in both air and nitrogen environments with the LB trough in a glovebox.

VSFG Spectroscopy. A detailed description of our "inverted" broadband SFG (BB-SFG) experiment was published elsewhere.[26] Briefly, the BB-SFG setup is based on a Ti:sapphire femtosecond oscillator and a femtosecond Ti:sapphire regenerative amplifier (Coherent, Legend) that produce 80 fs, 800 nm pulses at a 1 kHz repetition rate. Approximately 400 μJ of the Ti:Sa fundamental was used to pump a femtosecond optical parametric amplifier (Light-Conversion TOPAS), producing signal (*S*, 1300 nm) and idler (*I*, 2080 nm) outputs. Signal and idler were spatially separated, rotated, and then recombined for non-colinear difference frequency mixing in a 1.2 mm $AgGaS_2$ crystal, producing broad bandwidth (∼150 cm^{-1} fwhm) femtosecond IR pulses centered around 2900 cm^{-1}. The residual signal *S* (∼30 μJ) was separated from the idler *I* and femtosecond IR signals and was used to produce narrow bandwidth "inverted" picosecond visible pulses (centered at ∼650 nm) by second harmonic generation in a long $LiNbO_3$ crystal (2 cm long, θ = 58.9°). Sum mixing at the sample with the inverted visible pulse offers the best combination of spectral resolution and sensitivity in BB-SFG.[26]

The synchronized femtosecond IR pulses and picosecond visible pulses were spatially and temporally overlapped at the horizontal sample surface. The incidence angles for visible and IR beams were ∼62° and ∼60°, respectively, from surface normal. The beams were independently focused using two lenses, (f = 50 mm, CaF_2 for IR and f = 25 mm, BK7 for visible, with beam diameters of ∼8 and ∼6 mm for IR and visible, respectively). For systems of biological interest, optical damage by the intense femtosecond laser pulses is a concern. Therefore, low laser pulse energies at the sample were implemented: ∼1.7 μJ/pulse for the femtosecond IR and ∼3 μJ/pulse for the picosecond visible. Large focal spot sizes, 250 μm for the IR (3.4 mJ/

dx.doi.org/10.1021/la301332e | *Langmuir* 2012, 28, 12999−13007

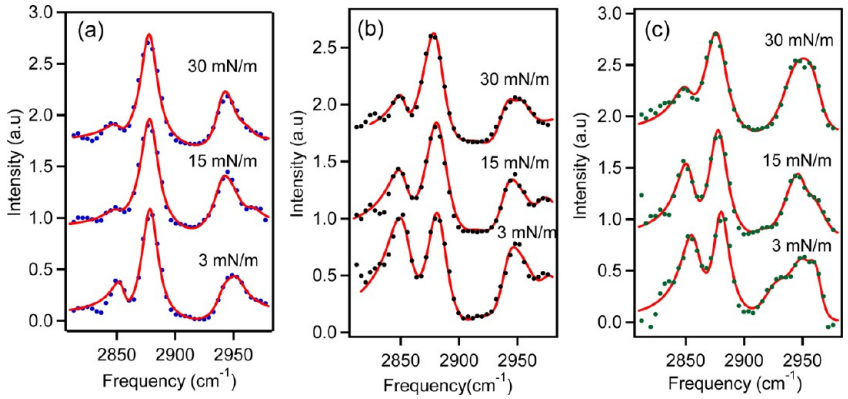

Figure 1. VSFG spectra recorded using an SSP polarization combination for SM monolayers deposited on glass at different surface pressures: (a) ESM, (b) BSM, and (c) MSM. Experimental data are shown as points and fits as solid lines. The relative intensities of the CH_2 ss and CH_3 ss signals provide information on the orientational order and extent of gauche defects for the acyl chains.

cm^2 fluence) and 150 μm for the visible, were used in order to minimize potential damage and/or heating effects at the sample. The heat-induced disordering of monolayers due to resonant absorption (most likely by water) of the femtosecond IR has been reported.[27] For the dry transferred monolayers and relatively low IR fluence used in the present studies, heating effects are minimized. This is confirmed by the fact that the recorded SFG spectra were independent of integration time or location within the sample. The polarization of the visible light was controlled by a Berek's polarization compensator (BC) while the polarization of IR was set to be vertical using a periscope. The IR spectral resolution in our inverted BB-SFG scheme is determined by the bandwidth of the upconverting visible pulse, in the present case, 7 cm^{-1}. The SFG signal from the sample surface was recollimated and spectrally filtered, passing through a 300 mm monochromator (Acton Spectra-Pro 300i) before being detected by a cooled (−40 °C) nanosecond gated intensified CCD camera (Princeton Instruments PI-MAX: 1024 Unigen II, 1024 × 256 pixels). We used a 200 ns gate to minimize background light. For data acquisition, 8 pixel horizontal binning on the CCD chip was applied to further increase signals. Data acquisition times for SFG spectra were typically 20 min. To optimize the resonant signals while simultaneously suppressing the nonresonant background, an IR-visible time delay of ∼1.5 ps was used.[26,28−30]

Spectral Line Shape Fitting. The intensity of the SFG signal is governed by the second order nonlinear susceptibility, $\chi^{(2)}_{SFG}$, which is related to the intensity of incident IR and visible light by the following equation:

$$I_{SFG}(\omega_{IR}) \propto |\chi^{(2)}_{SFG}(\omega_{IR})|^2 I_{IR}(\omega_{IR}) I_{vis}(\omega_{vis}) \quad (1)$$

$I_{IR}(\omega_{IR})$ and $I_{vis}(\omega_{vis})$ are the intensity of the IR and visible light, respectively. The $\chi^{(2)}_{SFG}$ can be represented by coherently summed Lorentzian functions

$$\chi^{(2)}_{SFG}(\omega_{SFG}) = a_{NR}\, e^{i\phi} + \sum_{\nu=1}^{n} \frac{b_\nu \Gamma_\nu}{\omega_{IR} - \omega_\nu + i\Gamma_\nu} \quad (2)$$

where b_ν and Γ_ν are the amplitude and line width of the resonant νth vibrational transition mode, a_{NR} is the amplitude of the nonresonant contribution, and ϕ is the phase difference between the resonant and nonresonant terms. Although the intensities of the SFG signals varied with the square of the number of coherent oscillators and, hence, with the surface pressure at which the monolayers were transferred, we report here only normalized spectra. Tables of the fitting parameters for the various spectra are provided in the Supporting Information.

Atomic Force Microscopy. AFM images were obtained in air at room temperature (22 ± 1 °C) using a PicoSPM atomic force microscope (Molecular Imaging) in MAC (magnetic alternating current) mode. A 30 × 30 μm^2 scanner operated at a scan rate between 0.7 and 1.3 Hz and type II MAC levers with spring constant of ∼2.8 N/m were used. The images shown are flattened raw data. Height differences between monolayer phases were determined from histograms of representative images.

RESULTS

Monolayers of the three natural SMs and their mixtures with Chol were prepared by Langmuir−Blodgett transfer from the air−water interface. Literature isotherms for synthetic SMs with saturated acyl chains exhibit a plateau between 10 and 20 mN/m (depending on the acyl chain length) that is indicative of a region of coexisting liquid expanded (l_e, disordered) and liquid condensed (l_c, ordered) phases.[31] This transition between l_c and l_e phases is detected as a small shoulder in the isotherms for ESM (Figure S1), despite the heterogeneous distribution of acyl chain lengths, and in agreement with literature results.[11] However, the transition is no longer observable for BSM which has a relatively high fraction of unsaturated acyl chains (21% C24:1 in our experiments); note that variation in the acyl chain length and saturation between different batches and sources of BSM may result in slight differences in the measured isotherms.[10,11] Interestingly, the distinct shoulder consistent with the l_e–l_c transition is still apparent for MSM (Figure S1) even though it has the most heterogeneous distribution of acyl chains.

Addition of 10 and 25 mol % Chol condensed the SM monolayers, as evidenced by the shift to smaller area per molecule (Figure S1), and as reported previously;[10,11,32] the ability of Chol to condense SM monolayers is somewhat less for the natural SMs than for pure synthetic SMs. Monolayers of mixtures of Chol with the three natural SMs were transferred to glass at three surface pressures for VSFG studies; this pressure range was selected to include samples with coexisting l_e and l_c phases at low surface pressure and more uniform monolayers with predominantly the l_c phase at high surface pressure. Selected samples were transferred to either glass or mica for examination of their morphologies by AFM.

VSFG Spectra of Sphingomyelin Monolayers. VSFG spectra were recorded for SM monolayers using an SSP polarization combination: S-SFG, S-vis, and P-IR. The broad-band IR was centered at 2900 cm^{-1}, and all spectra were ratioed to the IR pulse spectrum recorded using the nonresonant signal from a GaAs surface. Note that all VSFG spectra reported here are intensity normalized to the large 2880 cm^{-1} peak (CH_3 ss). The intensities for the various spectra are therefore relative to the CH_3 ss peak for each case. The VSFG spectra for ESM shown in Figure 1a display two peaks at ∼2850 and ∼2880

dx.doi.org/10.1021/la301332e | Langmuir 2012, 28, 12999−13007

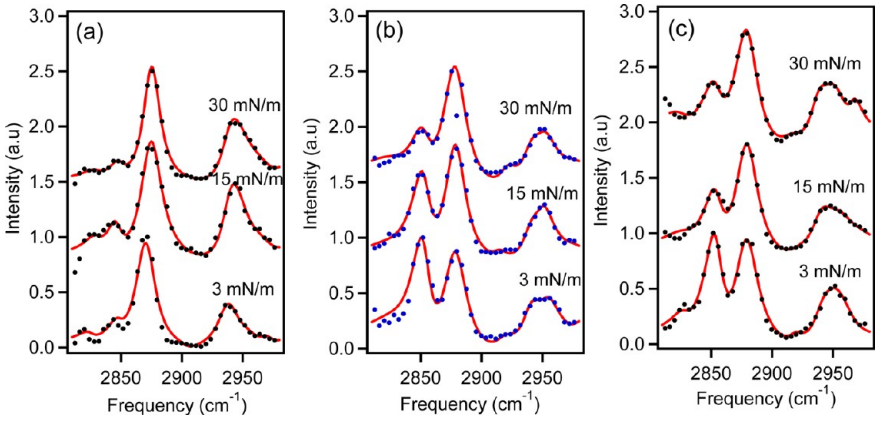

Figure 2. VSFG spectra recorded using an SSP polarization combination for SM + 10 mol % Chol-d_7 monolayers deposited on glass at different surface pressures: (a) ESM, (b) BSM, and (c) MSM. Experimental data are shown as points and fits as solid lines.

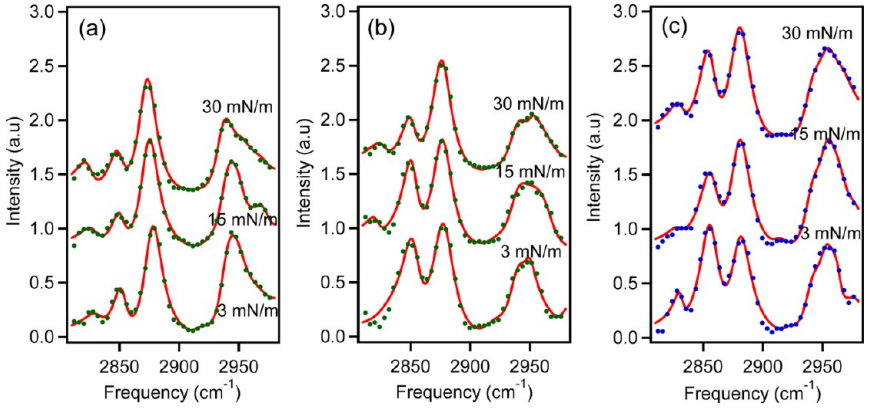

Figure 3. VSFG spectra recorded using an SSP polarization combination for SM + 25 mol % Chol-d_7 monolayers deposited on glass at different surface pressures: (a) ESM, (b) BSM, and (c) MSM. Experimental data are shown as points and fits as solid lines.

cm^{-1} corresponding to the CH_2 symmetric stretch (CH_2 ss) and CH_3 symmetric stretch (CH_3 ss); the broad peak at ~2950 cm^{-1} is a combination of the CH_3 Fermi resonance (typically 2936 cm^{-1}) and the CH_3 asymmetric stretch (CH_3 as).[22,33,34] At each of the surface pressures examined (3, 15, 30 mN/m), the intensity of the CH_3 ss was much higher than that of the CH_2 ss transition, indicating that ESM forms well packed monolayers with few gauche conformations in the lipid chains. Changes in surface pressure have only a modest effect on the conformational order, with a slightly stronger CH_2 stretch transition at the lowest surface pressure of 3 mN/m. These results demonstrate that ESM forms a highly ordered lipid monolayer even at low surface pressures, despite its heterogeneous composition (86% C16:0 SM with the remaining 14% a mixture of long-chain saturated and unsaturated SMs).

In Figure 1b, we show the VSFG spectra of BSM monolayers deposited at 3, 15, and 30 mN/m surface pressure. In contrast with the results for ESM monolayers, CH_2 ss and CH_3 ss signal intensities are similar at low surface pressures, indicating significant conformational disorder. The CH_2 ss signal decreases with increasing surface pressure, consistent with a decreasing contribution of gauche conformations in the lipid chains for the more tightly packed monolayers. The VSFG spectra of MSM monolayers shown in Figure 1c show a similar trend to those for BSM, with a strong CH_2 ss contribution at low surface pressures. The CH_2 ss signal also decreases with increasing surface pressure, although to a lesser extent than for BSM. VSFG spectra for BSM monolayers have the largest contribution from the CH_2 ss transition of the three SMs at low surface pressure.

VSFG Spectra for Sphingomyelin–Cholesterol Monolayers. Several groups have reported VSFG studies of DPPC/Chol monolayers, providing information on the changes in conformation and orientational order of the monolayers as a function of surface pressure and Chol content.[21,22,25,27] VSFG spectra of SM monolayers containing 10 and 25 mol % Chol as a function of surface pressure are provided in Figures 2 and 3. Cholesterol-d_7 was used for this study in order to minimize contributions from Chol in the CH stretch region.[24] Previous studies have shown that there is negligible contribution from Chol-d_7 in the CH_3 ss region (2880 cm^{-1}), weak signals in the CH_2 ss region (2850 cm^{-1}) and at 2820 cm^{-1}, and strong signals between 2900 and 3000 cm^{-1} in the CH_3 as region.[22,24,25] The VSFG spectrum for a Chol-d_7 monolayer transferred at 15 mN/m (Figure S2) is in good agreement with this literature data.[22,24,25] VSFG spectra of 9:1 ESM/Chol-d_7 monolayers deposited at 3, 15, and 30 mN/m are shown in Figure 2a. The spectra in the 2800–2900 cm^{-1} region are very similar to those obtained for ESM alone, with a strong CH_3 ss signal and very weak signals in the CH_2 ss region, indicating that Chol has little effect on the already well-ordered ESM monolayer. VSFG spectra for monolayers with 25 mol % Chol-d_7 (Figure 3a) show a more intense peak at 2950 cm^{-1} and a new weaker signal at 2820 cm^{-1}, which appears to be due to Chol-d_7, based on the spectrum of a pure Chol-d_7 monolayer.

dx.doi.org/10.1021/la301332e | Langmuir 2012, 28, 12999–13007

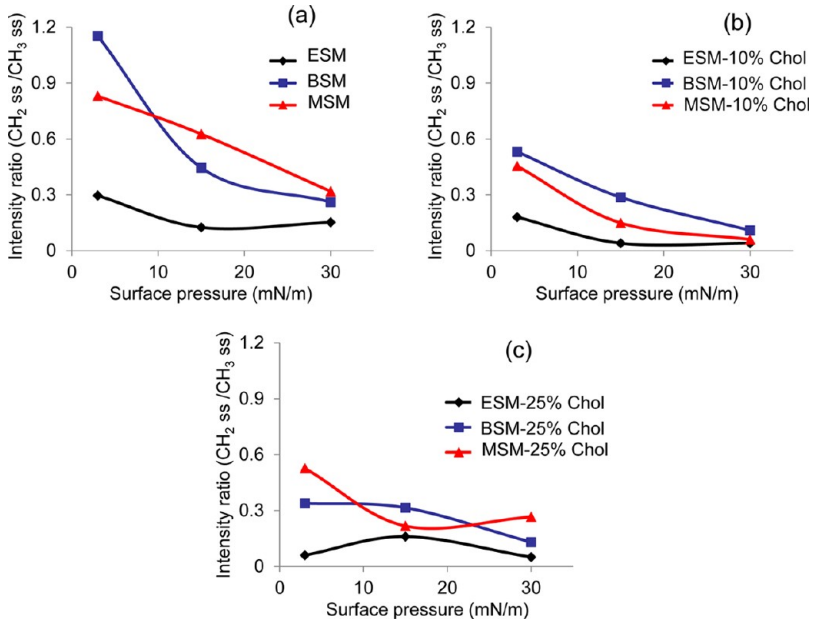

Figure 4. Corrected CH_2 ss/CH_3 ss intensity ratios for SM monolayers as a function of surface pressure and Chol concentration: (a) ESM, BSM, and MSM monolayers; (b) SM + 10 mol % Chol; and (c) SM + 25 mol % Chol.

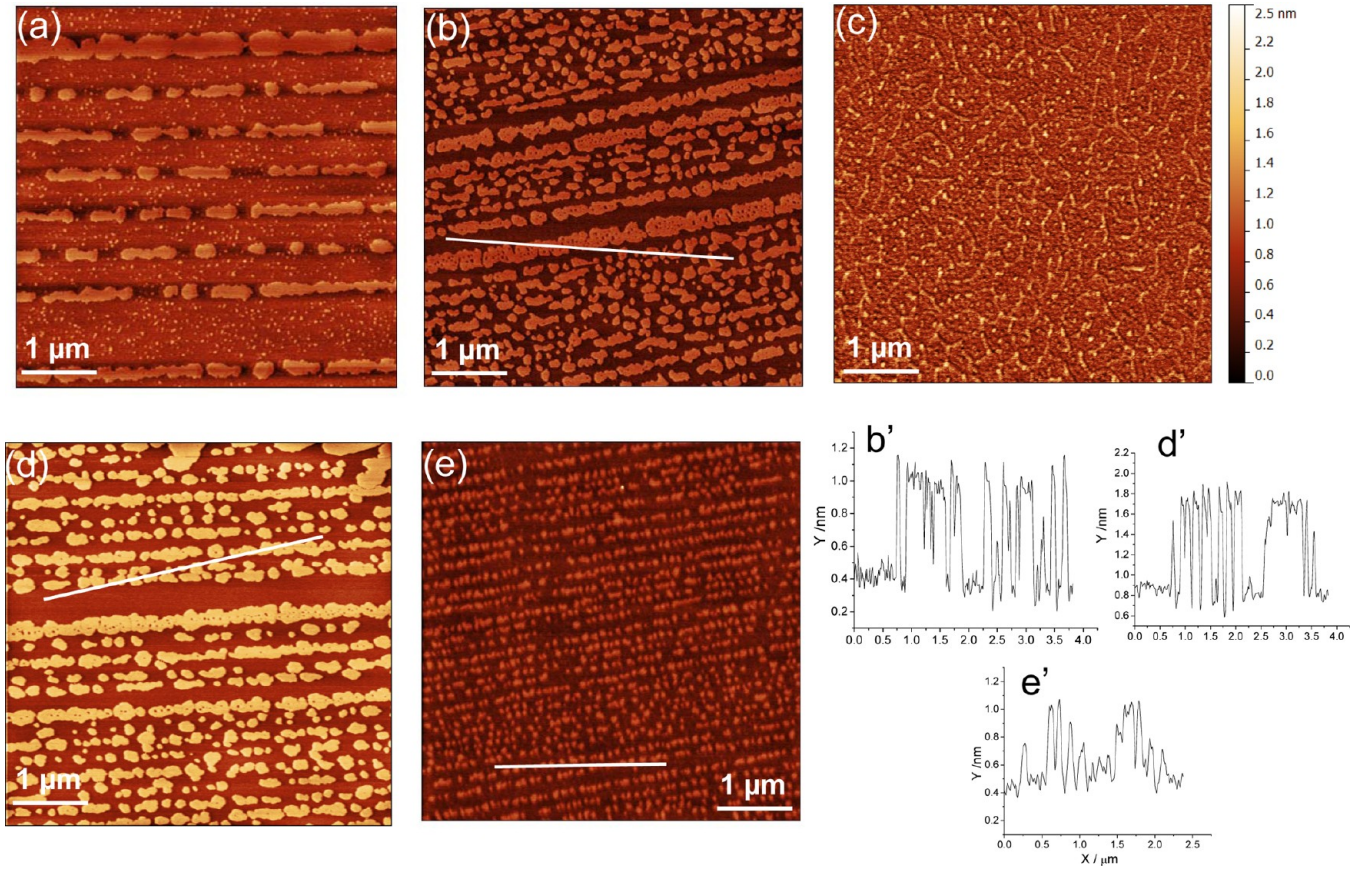

Figure 5. AFM images for SM monolayers transferred to mica at various surface pressures: (a–c) ESM monolayers transferred at 3, 15, and 30 mN/m; (d, e) BSM and MSM monolayers transferred at 15 mN/m; (e) cross sections for the lines marked in b, d and e are labeled b′, d′ and e′, respectively. All images are displayed on the same *z*-scale.

Based on the relative intensities of the 2820 and 2850 cm^{-1} signals for ESM-Chol-d_7 and pure Chol-d_7, we conclude that most of the signal at 2850 cm^{-1} is due to Chol-d_7 rather than to gauche conformers of the SM alkyl chains, consistent with a well-ordered monolayer. Spectra of BSM and MSM monolayers containing 10 mol % Chol-d_7 showed significant CH_2 ss vibrational stretches for all three surface pressures, with a decreasing contribution relative to the CH_3 ss transition with

dx.doi.org/10.1021/la301332e | *Langmuir* 2012, 28, 12999–13007

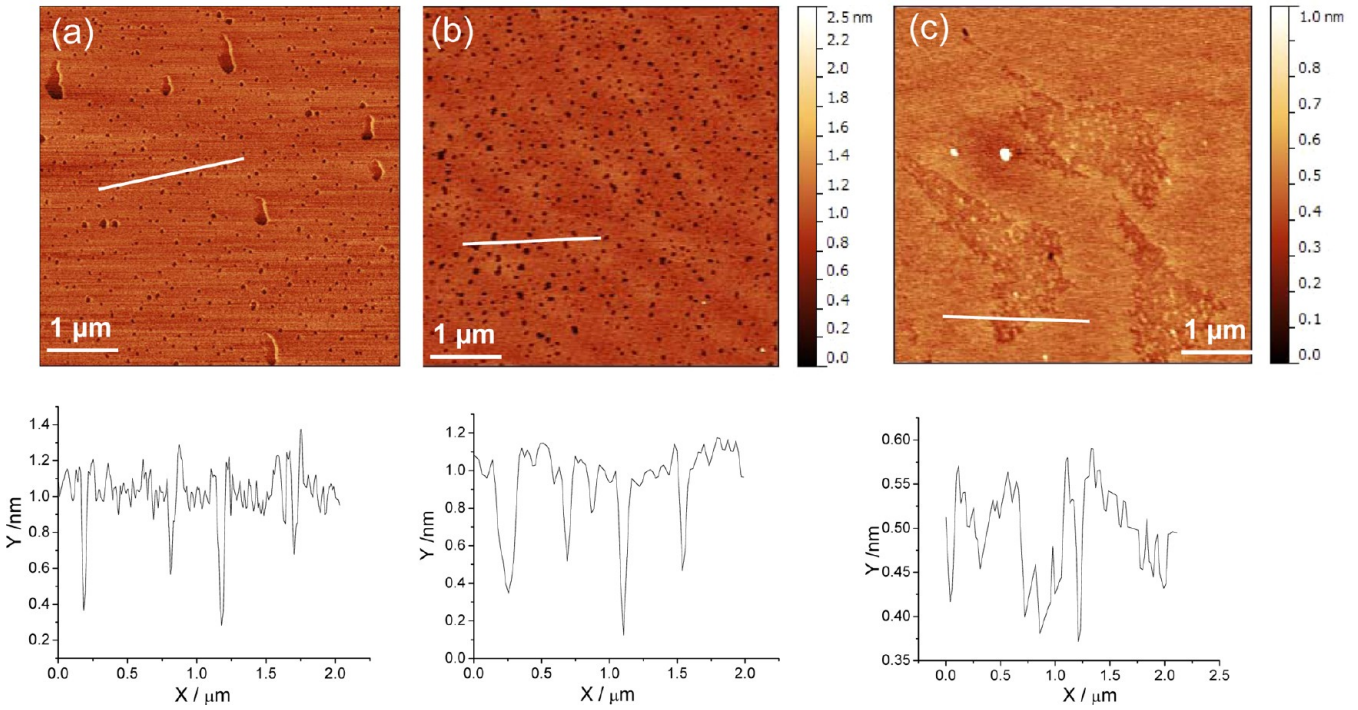

Figure 6. AFM images for SM + 25 mol % Chol monolayers transferred at 15 mN/m: (a) ESM, (b) BSM, and (c) MSM. Cross sections are shown for the lines marked on each image. Note the smaller *z*-scale for image c compared to a and b.

increasing surface pressure. Larger contributions from the CH_2 ss transitions were observed for monolayers with 25 mol % Chol-d_7.

A spectral line shape fitting procedure was used to extract the intensities of the CH_2 and CH_3 symmetric stretches for the various SM and SM-Chol-d_7 monolayers. The CH_2/CH_3 intensity ratio then provides an estimate of the magnitude of gauche conformations in the SM acyl chains. The contribution of Chol-d_7 to the CH_3 symmetric stretch at 2880 cm^{-1} is negligible since the two terminal methyl groups are deuterated; however, the contribution from Chol-d_7 to the CH_2 ss transition is non-negligible in the VSFG spectra for the mixed monolayers, as noted above. Since VSFG spectroscopy is a coherent process, the complex amplitudes of the transitions are coherently added before being squared at the detector. For data analysis, we neglected the phase difference of Chol-d_7 and SM molecules and considered the total CH_2 ss intensity of the mixture as the sum of the individual CH_2 ss intensities from SM and Chol-d_7. Chol-d_7 produces a unique transition at 2820 cm^{-1} previously assigned to an unspecified ring CH_2 symmetric stretch.[22,35] We measured the intensity ratio for the 2820 and 2850 cm^{-1} transitions from the VSFG spectrum for a pure Chol-d_7 monolayer deposited at 15 mN/m surface pressure (Figure S2). The corrected CH_2 ss intensity (due to only SM)[21] was estimated for the SM-Chol-d_7 mixtures using the fitting results and taking into account the 2820/2850 cm^{-1} intensity ratio for pure Chol-d_7, assuming the intensity ratios are the same for SM-Chol-d_7 mixtures at different surface pressures.

The extracted intensity ratios (CH_2 ss/CH_3 ss) for ESM, BSM and MSM as a function of surface pressure are shown in Figure 4a. The intensity ratio for ESM is smaller than those for BSM and MSM at each surface pressure, indicating a higher degree of alignment for the ESM acyl chains and a considerably larger fraction of gauche conformations for both BSM and MSM. Addition of Chol has a significant effect on the degree of order of acyl chains for both BSM and MSM, particularly at low surface pressure, as can be seen in Figure 4b and c. By contrast, it has a relatively modest effect on ESM, which already has small contributions from gauche defects over the entire pressure range examined.

AFM for Sphingomyelin and Sphingomyelin–Cholesterol Monolayers. Monolayers of the three natural SMs were transferred to mica at several surface pressures and imaged by AFM for correlation with the VSFG data. Each SM monolayer exhibited phase separation at low surface pressures (3 and 15 mM/m), as illustrated in Figures 5 and S3. For example, ESM monolayers had small aligned and interconnected l_c domains at both 3 and 15 mN/m with a larger fraction of the higher phase at the higher surface pressure (Figure 5a, b; domains are 0.4 and 0.7 nm above the surrounding monolayer, respectively). Note that alignment of domains has been shown to occur during transfer from the air–water interface for a number of phase separated monolayers.[36] At the highest surface pressure used (30 mN/m), the ESM monolayer was more uniform with a small fraction of thin lines of a higher phase (Figure 5c). Similar results were obtained for the other two SMs, as illustrated by images for monolayers transferred at 15 mN/m (Figure 5 d, e) which had small aligned domains that were 0.9 (BSM) and 0.5 nm (MSM) above the surrounding monolayer and by additional images for BSM in Figure S3a, b. The results for ESM and BSM agree well with earlier AFM and fluorescence studies which demonstrated that C_{16}-SM and BSM monolayers exhibit a mixture of coexisting l_c and l_e phases below 20 mN/m surface pressure;[37−39] at 30 mN/m, BSM monolayers were predominantly in the l_c phase with only small areas of the lower l_e phase, very similar to our observations (Figure S3b).[38] The presence of phase separation for MSM is somewhat surprising, given the larger heterogeneity in the acyl

dx.doi.org/10.1021/la301332e | *Langmuir* 2012, 28, 12999−13007

chain lengths, with the major component being 34% C23:0 but with ∼20% each of C22:0 and C24:0.

Addition of Chol to ESM monolayers has been shown to abolish the l_e/l_c phase transition, with the point at which the transition disappears varying with % Chol and surface pressure.[37,40] Based on the literature results, one would predict uniform homogeneous monolayers above ∼10 mN/m for lipid mixtures with 10−25 mol % Chol. Consistent with this hypothesis, ESM and BSM monolayers containing 25 mol % Chol and transferred at 15 mN/m gave uniform monolayers with occasional small depressions that were ∼0.6 nm lower in height (Figure 6a, b). In contrast with these results, MSM monolayers containing 25% Chol still showed clear phase separation (Figure 6c), although the height difference between the two phases was only 0.2 nm, considerably less than that for MSM monolayers. Cholesterol-containing monolayers showed clear phase separation to give large condensed domains surrounded by a small amount of l_e phase at 3 mN/m and a reasonably uniform monolayer with thin lines of a higher phase at 30 mN/m, as shown for representative ESM monolayers containing 25 mol % Chol in Figure S3c and d.

In several cases, monolayers transferred to the same glass slides used for VSFG experiments were imaged by AFM. However, the surface roughness of the glass was significantly higher than that of mica, making it difficult to clearly resolve the small domains observed on mica for some samples. In order to compare AFM and VSFG results for samples on the same support, monolayers of the three SMs and their mixtures with 25% Chol were transferred to mica at 15 mN/m and examined by VSFG (Figure S4). Although the spectra on mica were complicated by the presence of strong nonresonant contributions from the mica support for part of the CH region (>2950 cm^{-1} and <2840 cm^{-1}), the results over a narrower frequency range were qualitatively similar to those obtained on glass substrates. The ESM spectra had minimal contributions from gauche defects, whereas spectra for both BSM and MSM had similar intensities for the CH_2 ss and CH_3 ss transitions, indicative of significant conformational disorder. For ESM monolayers with 25% Chol, the CH_2 ss transition was also of low intensity, whereas similar CH_2 ss and CH_3 ss transition intensities were observed for BSM and MSM. These results indicate that qualitatively similar results are obtained on the two supports, although mica is not ideal for VSFG studies due to nonresonant contributions in the CH stretch region.

As an additional control experiment, we tested whether lipid oxidation had an effect on the observed monolayer morphologies.[41−46] Since BSM contains the largest amount of unsaturated acyl chains and would be the most susceptible to oxidation, we initially compared monolayer morphologies for BSM monolayers prepared in nitrogen and air environments. As shown in Figure S5, monolayers transferred at 15 mN/m had occasional large domains that were not observed for monolayers transferred in a nitrogen environment. Nevertheless, clear phase separation was obtained for both samples, suggesting that lipid oxidation is not a major issue for these monolayers. BSM monolayers containing 25 mol % Chol had smaller areas of the lower phase when samples were prepared in a nitrogen atmosphere (Figure S6a and b). Differences in the fraction of lower phase were also observed for ESM monolayers prepared under air and nitrogen and transferred at 15 mN/m (Figure S6c and d).

DISCUSSION

The VSFG spectra measured for ESM monolayers over the 3−30 mN/m surface pressure range provide evidence for well-ordered monolayers in which the acyl chains have a high degree of conformational order, with few gauche defects. Monolayers of the more heterogeneous BSM and MSM have significantly larger CH_2/CH_3 intensity ratios than do ESM monolayers at low surface pressures (3 and 15 mN/m), consistent with a larger fraction of gauche conformers. The increased contribution from gauche defects for BSM reflects the presence of >20% unsaturated acyl chains. However, MSM has a much lower level of unsaturation than BSM (<5%, similar to ESM); in this case, the higher contribution of gauche defects is consistent with lipid disorder caused by the significantly more heterogeneous acyl chain length distribution (from C16 to C24), rather than by kinks associated with double bonds. A previous SFG study of saturated PC monolayers has shown that the contribution from gauche defects decreases significantly when the acyl chain length increases from C14 to C18.[47] The increased disorder for MSM compared to ESM monolayers clearly demonstrates that the heterogeneity of the acyl chain lengths dominates over the anticipated increase in monolayer order due to the longer acyl chains. Interestingly, the difference between the CH_2/CH_3 intensity ratios for the three natural SM mixtures is much smaller at high surface pressure, consistent with conformationally ordered lipid tails at pressures similar to those obtained in bilayer membranes.

AFM images for the three natural SMs show coexisting l_e and l_c phases at 3 and 15 mN/m, while more uniform monolayers with only a small fraction of higher phase are obtained at 30 mN/m. We emphasize that the small and/or interconnected raised domains observed by AFM for the SM monolayers would not be detected by epifluorescence. The AFM images also demonstrate the absence of small surface defects, which would have disordered lipids around their perimeters. The decrease in gauche conformers as the monolayer is compressed from 15 to 30 mN/m for BSM and MSM may reflect the conversion of the l_e phase to the more tightly packed l_c phase. By contrast, for ESM, there is a more modest effect of increased surface pressure, consistent with both l_e and l_c phases having conformationally well-ordered acyl chains.

Previous studies of DPPC monolayers at the air−water interface have reported that the VSFG spectra at low surface pressure (3 mN/m) are dominated by the CH_2 ss signal, indicating a conformationally disordered monolayer with many gauche defects.[21,25] However, a recent report demonstrated that the ratio of CH_2 ss to CH_3 ss signals is strongly dependent on the fluence of the IR laser.[27] The CH_2 signal is readily detectable at high laser fluence, but disappears for low fluence, whereas the CH_3 signal increases in intensity at low laser fluence. This provides clear evidence that resonant sample heating by the IR laser beam leads to disordered acyl chains and indicates that the steady state heating is sufficient to increase the sample temperature above the DPPC phase transition temperature (T_M = 41 °C).[27] Laser heating is much less likely to be a problem for VSFG experiments on dry monolayers on glass slides, consistent with the observation that our spectra are independent of integration (exposure) time. Furthermore, our VSFG results indicate well-ordered monolayers for ESM, confirming that the significant disorder observed for BSM and MSM is unlikely to be caused by laser heating effects. In addition to minimizing laser heating effects, the transferred

dx.doi.org/10.1021/la301332e | Langmuir 2012, 28, 12999−13007

monolayers have the advantage of compatibility with AFM measurements for correlation of sample morphology with monolayer order as assessed by VSFG.

Although the changes in conformational order for the SM monolayers are consistent with expectations based on the acyl chain heterogeneity and the AFM results, it is important to consider whether lipid oxidation contributes to the sample disorder. Control experiments in which monolayers were prepared in air vs nitrogen environments showed modest changes in the extent of l_c and l_e phases for BSM, the lipid with the largest fraction of unsaturated acyl chains, and a somewhat smaller effect for ESM. This is in contrast to studies of ternary lipid mixtures where oxidized lipids were shown to significantly modify the miscibility transition pressure, leading to stable domains over a wider pressure range.[46] For example, addition of 7.5 mol % of an oxidized lipid was shown to increase the miscibility transition from ∼10 mN/m to ∼32 mN/m. Lipid oxidation at the air water interface is particularly efficient for poly unsaturated lipids, but is considerably slower for lipids with a single double bond.[42,43] For example, monounsaturated lipids such as POPC show minimal oxidation-induced changes under ambient conditions at the air−water interface over a period of ∼30 min.[42,45] Furthermore, lipid oxidation is considerably slower at higher surface pressure, suggesting that even if oxidation does contribute to monolayer disorder at low surface pressure it will be much less of an issue at high surface pressure.[43] Although we have observed that oxidation at the air−water interface leads to changes in domain morphology as assessed by AFM for some ternary lipid mixtures, storing monolayers in air vs nitrogen did not lead to further changes, indicating that oxidation during the SFG experiments on dry monolayers is unlikely to be a problem.[41] Taken together, the above considerations suggest that although lipid oxidation may contribute to some additional disorder in SM monolayers, especially at low surface pressure and for BSM, it is unlikely to be the main source of conformational disorder in these monolayers.

The addition of Chol has a relatively small effect on the ESM monolayers, which are already well-ordered over the range of surface pressures that we have examined. However, Chol has a more pronounced effect on BSM and MSM monolayers at low surface pressures. It is particularly interesting that the addition of Chol can overcome the disorder introduced by the presence of a heterogeneous mixture of acyl chains and, in the case of BSM, the presence of a significant fraction of unsaturated chains. In fact, at 30 mN/m all three SMs have relatively low CH_2/CH_3 intensity ratios, consistent with a similar level of conformational ordering and a relatively low fraction of gauche defects in the lipid tails in both the absence and presence of Chol. This suggests that the ability of SM to act as both a hydrogen bond donor and acceptor leads to increased hydrogen bonding interactions which affect the conformational order in both SM and SM/Chol mixtures.

As discussed in several recent reviews,[5−7,48] a large number of experimental studies have provided evidence for a stronger interaction between Chol and SM than between Chol and a similar, chain-matched PC. Comparison with recent results for DPPC in which laser heating effects have been eliminated indicate that DPPC monolayers exhibit a high degree of conformational order even at low surface pressure,[27] and are thus unlikely to show large effects of Chol addition. A direct comparison of SM and PC mixtures under the same conditions and in the absence of laser heating effects would be required to investigate whether measurements of CH_2/CH_3 intensity ratios from VSFG spectra are diagnostic of the stronger interaction with Chol for SM as compared to PC. Independent of this, the SM results are particularly interesting in the context of the organization of the plasma membrane where sphingolipid−Chol domains are believed to play an important role in organizing proteins to amplify cell signaling.[1,8,9] The VSFG results presented here indicate that well-ordered lipid membranes are obtained for monolayers of Chol and natural SMs at a pressure similar to that within a cell membrane.

■ ASSOCIATED CONTENT

Supporting Information

Three figures with surface pressure isotherms for SM and SM-Chol monolayers, additional VSFG spectra for a pure Chol monolayer on glass and SM-Chol monolayers on mica and tables of fitting parameters for VSFG spectra. This material is available free of charge via the Internet at http://pubs.acs.org.

■ AUTHOR INFORMATION

Corresponding Author

*E-mails: Linda.Johnston@nrc-cnrc.gc.ca, Albert.Stolow@nrc-cnrc.gc.ca.

Notes

The authors declare no competing financial interest.

■ ACKNOWLEDGMENTS

A.S. and L.J.J. thank the Natural Sciences and Engineering Research Council for support.

■ REFERENCES

(1) Simons, K.; Gerl, M. J. Revitalizing membrane rafts: new tools and insights. *Nat. Rev. Mol. Cell Biol.* **2010**, *11*, 688−699.

(2) Johnston, L. J. Nanoscale imaging of domains in supported lipid membranes. *Langmuir* **2007**, *23*, 5886−5895.

(3) London, E. How principles of domain formation in model membranes may explain ambiguities concerning lipid raft formation in cells. *Biochim. Biophys. Acta* **2005**, *1746*, 203−220.

(4) Veatch, S. L.; Keller, S. L. Seeing spots: Complex phase behavior in simple membranes. *Biochim. Biophys. Acta* **2005**, *1746*, 172−185.

(5) McMullen, T. P. W.; McElhaney, R. N. Physical studies of cholesterol-phospholipid interactions. *Curr. Opin. Colloid Interface Sci.* **1996**, *1*, 83−90.

(6) Rog, T.; Pasenkiewicz-Gierula, M.; Vattulainen, I.; Kartunnen, M. Ordering effects of cholesterol and its analogues. *Biochim. Biophys. Acta* **2009**, *1788*, 97−121.

(7) Ohvo-Rekila, H.; Ramstedt, B.; Leppimaki, P.; Slotte, J. P. Cholesterol interactions with phospholipids in membranes. *Prog. Lipid Res.* **2002**, *41*, 66−97.

(8) Simons, K.; Ikonen, E. Functional rafts in cell membranes. *Nature* **1997**, *387*, 569−572.

(9) Pike, L. J. Rafts defined: a report on the Keystone symposium on lipid rafts and cell function. *J. Lipid Res.* **2006**, *47*, 1597−1598.

(10) Smaby, J. M.; Brockman, H. L.; Brown, R. E. Cholesterol's interfacial interactions with sphingomyelins and phosphatidylcholines: Hydrocarbon chain structure determines the magnitude of condensation. *Biochemistry* **1994**, *33*, 9135−9142.

(11) Li, X.-M.; Momsen, M. M.; Smaby, J. M.; Brockman, H. L.; Brown, R. E. Cholesterol decreases the interfacial elasticity and detergent solubility of sphingomyelins. *Biochemistry* **2001**, *40*, 5954−5963.

(12) Ye, S.; Nguyen, K. T.; Le Clair, S. V.; Chen, Z. In situ molecular level studies on membrane related peptides and proteins in real time using sum frequency generation vibrational spectroscopy. *J. Struct. Biol.* **2009**, *168*, 61−77.

(13) Bredenbeck, J.; Ghosh, A.; Nienhuys, H.-K.; Bonn, M. Interface-specific ultrafast two-dimensional vibrational spectroscopy. *Acc. Chem. Res.* **2009**, *42*, 1332−1342.
(14) Chen, X.; Chen, Z. SFG studies on interactions between antimicrobial peptides and supported lipid bilayers. *Biochim. Biophys. Acta* **2006**, *1758*, 1257−1273.
(15) Kim, G.; Gurau, M. C.; Lim, S.-M.; Cremer, P. S. Investigations of the orientation of a membrane peptide by sum frequency spectrscopy. *J. Phys. Chem. B* **2003**, *107*, 1403−1409.
(16) Hill, K.; Penzes, C. B.; Schnoller, D.; Horvati, K.; Bosze, S.; Hudecz, F.; Keszthelyi, T.; Kiss, E. Characterization of the membrane affinity of an isoniazide peptide conjugate by tensiometry, atomic force microscopy and sum-frequency vibrational spectroscopy, using a Langmuir monolayer model. *Phys. Chem. Chem. Phys.* **2010**, *12*, 11498−11506.
(17) Liu, J.; Conboy, J. C. 1,2-Diacyl-phosphatidylcholine flip-flop measured directly by sum-frequency vibrational spectroscopy. *Biophys. J.* **2005**, *89*, 2522−2532.
(18) Anglin, T. C.; Liu, J.; Conboy, J. C. Facile lipid flip-flop in a phospholipid bilayer induced by gramicidin A measured by sum-frequency vibrational spectroscopy. *Biophys. J.* **2007**, *92*, L01−L03.
(19) Anglin, T. C.; Conboy, J. C. Kinetics and Thermodynamics of flip-flop in binary phospholipid membranes measured by sum-frequency vibrational spectroscopy. *Biochemistry* **2009**, *48*, 10220−10234.
(20) Fu, L.; Liu, J.; Yan, E. C. Y. Chrial sum frequency generation spectroscopy for characterizing protein secondary structures at interfaces. *J. Am. Chem. Soc.* **2011**, *133*, 8094−8097.
(21) Bonn, M.; Roke, S.; Berg, O.; Juurlink, L. B. F.; Stamouli, A.; Muller, M. A molecular view of cholesterol-induced condensation in a lipid monolayer. *J. Phys. Chem. B* **2004**, *108*, 19083−19085.
(22) Kett, P. J. N.; Casford, M. T. L.; Davies, P. B. Structure of mixed phosphatidylethanolamine and cholesterol monolayers in a supported hybrid bilayer membrane studied by sum frequency generation vibrational spectroscopy. *J. Phys. Chem. B* **2011**, *115*, 6465−6473.
(23) Levy, D.; Briggman, K. A. Cholesterol/phospholipid interactions in hybrid bilayer membranes. *Langmuir* **2007**, *23*, 7155−7161.
(24) Liu, J.; Conboy, J. C. Phase behavior of planar supported lipid membranes composed of cholesterol and 1,2-distearoyl-sn-glycerol-3-phosphocholine examined by sum-frequency vibrational spectroscopy. *Vib. Spectrosc.* **2009**, *50*, 106−115.
(25) Ohe, C.; Sasaki, T.; Noi, M.; Goto, Y.; Itoh, K. Sum frequency generation spectroscopic study of the condensation effect of cholesterol on a lipid monolayer. *Anal. Bioanal. Chem.* **2007**, *388*, 73−79.
(26) Weeraman, C.; Mitchell, S. A.; Lausten, R.; Johnston, L. J.; Stolow, A. Vibrational sum frequency generation spectroscopy using inverted visible pulses. *Opt. Express* **2010**, *18*, 11483−11494.
(27) Backus, E. H. G.; Bonn, D.; Cantin, S.; Roke, S.; Bonn, M. Laser-heating-induced displacement of surfactants on the water surface. *J. Phys. Chem. B* **2012**, *116*, 2703−2712.
(28) Lagutchev, A.; Hambir, S. A.; Dlott, D. D. Nonresonant background suppression in broadband vibrational sum-frequency generation spectroscopy. *J. Phys. Chem. C* **2007**, *111*, 13645−13647.
(29) Curtis, A. D.; Reynolds, S. B.; Calchera, A. R.; Patterson, J. E. Understanding the fole of nonresonant sum-frequency generation from polystyrene thin films. *J. Phys. Chem. Lett.* **2010**, *1*, 2435−2439.
(30) Stiopkin, I. V.; Jayathilake, H. D.; Weeraman, C.; Benderskii, A. V. Temporal effects on spectroscopic line shapes, resolution, and sensitivity of the broad-band sum frequency generation. *J. Chem. Phys.* **2010**, *132*, 234503.
(31) Li, X.-M.; Smaby, J. M.; Momsen, M. M.; Brockman, H. L.; Brown, R. E. Sphingomyelin interfacial behavior: The impact of changing acyl chain composition. *Biophys. J.* **2000**, *78*, 1921−1931.
(32) Note that an *x*-axis of apparent molecular area is used for isotherms of SM-Chol mixtures in ref 10, which differs from the average molecular area used in this work (Figure S1) and in ref 11.
(33) Liu, J.; Conboy, J. C. Structure of a gel phase lipid bilayer prepared by the Langmuir-Blodgett/Langmuir-Schaefer method characterized by sum-frequency vibrational spectroscopy. *Langmuir* **2005**, *21*, 9091−9097.
(34) Roke, S.; Schins, J.; Muller, M.; Bonn, M. Vibrational spectroscopic investigation of the phase diagram of a biomimetic lipid membrane. *Phys. Rev. Lett.* **2003**, *90*, 128101.
(35) Bulkin, B. J.; Krishnan, K. Vibrational spectra of liquid crystals. III. Raman spectra of crystal, cholesteric and isotropic cholesterol esters, 2800−3100 cm^{-1} region. *J. Am. Chem. Soc.* **1971**, *93*, 5998−6004.
(36) Moraille, P.; Badia, A. Nanoscale stripe patterns in phospholipid bilayers formed by the Langmuir−Blodgett technique. *Langmuir* **2003**, *19*, 8041−8049.
(37) Kuikka, M.; Ramstedt, B.; Ohvo-Rekila, H.; Turf, J.; Slotte, J. P. Membrane properties of D-erythro-*N*-acyl sphingomyelins and their corresponding dihydro derivatives. *Biophys. J.* **2001**, *80*, 2327−2337.
(38) Milhiet, P. E.; Domec, C.; Giocondi, M.-C.; Mau, N. V.; Heitz, F.; Le Grimellec, C. Domain formation in models of the renal brush border membrane outer leaflet. *Biophys. J.* **2001**, *81*, 547−555.
(39) Yuan, C.; Furlong, J.; Burgos, P.; Johnston, L. J. The size of lipid rafts: An atomic force microscopy study of ganglioside GM1 domains in sphingomyelin/DOPC/cholesterol membranes. *Biophys. J.* **2002**, *82*, 2526−2535.
(40) Slotte, J. P. Lateral domain formation in mixed monolayers containing cholesterol and dipalmitoylphosphatidylcholine or *N*-palmitoylsphingomyelin. *Biochim. Biophys. Acta* **1995**, *1235*, 419−427.
(41) Coban, O.; Popov, J.; Burger, M.; Vobornik, D.; Johnston, L. J. Transition from nanodomains to microdomains induced by exposure of monolayers to air. *Biophys. J.* **2007**, *92*, 2842−2853.
(42) Liljeblad, J. F. D.; Bulone, V.; Tyrode, E.; Rutland, M. W.; Johnson, C. M. Phospholipid monolayers probed by vibrational sum frequency spectroscopy: Instability of unsaturated phospholipids. *Biophys. J.* **2010**, *98*, L50−L52.
(43) Tyrode, E.; Niga, P.; Johnson, M.; Rutland, M. W. Molecular structure upon compression and stability toward oxidation of langmuir films of unsaturated fatty acids: A vibrational sum frequency spectroscopy study. *Langmuir* **2010**, *26*, 14024−14031.
(44) Stottrup, B. L.; Stevens, D. S.; Keller, S. L. Miscibility of ternary mixtures of phospholipids and cholesterol in monolayers and application to bilayer systems. *Biophys. J.* **2005**, *88*, 269−276.
(45) Lai, C. C.; Tang, S. H.; Finlayson-Pitts, B. J. Interactions of monolayers of unsaturated phosphatidylcholines with ozone at the air-water interface. *Langmuir* **1994**, *10*, 4637−4644.
(46) Volinsky, R.; Paananen, R.; Kinnunen, P. K. J. Oxidized phosphatidylcholines promote phase separation of cholesterol-sphingomyelin domains. *Biophys. J.* **2012**, *103*, 247−254.
(47) Watry, M. R.; Tarbuck, T. L.; Richmond, G. L. Vibrational sum-frequency studies of a series of phospholipid monolayers and the associated water structure at the vapor/water interface. *J. Phys. Chem. B* **2003**, *107*, 512−518.
(48) Ramstedt, B.; Slotte, J. P. Sphingolipids and the formation of sterol-enriched ordered membrane domains. *Biochim. Biophys. Acta* **2006**, *1758*, 1945−1956.